*Materials Transactions*, Vol. 48, No. 7 (2007) pp. 1919 to 1923


# Microstructure and Electrical Conductivity of Epitaxial $BaRuO_3$ Thin Films Prepared on (001), (110) and (111) $SrTiO_3$ Substrates by Laser Ablation

Akihiko Ito*, Hiroshi Masumoto and Takashi Goto

*Institute for Materials Research, Tohoku University, Sendai 980-8577, Japan*

$BaRuO_3$ (BRO) thin films were prepared on $SrTiO_3$ (STO) single crystal substrate by laser ablation, and their microstructures and the anisotropy of electrical conductivity were investigated. The (205) and (104) doubly oriented BRO thin film was grown epitaxially on (001) STO substrate. Epitaxial (110) and (009) BRO thin films were obtained on (110) and (111) STO substrates, respectively, at oxygen pressure of 13 Pa and substrate temperature of 973 K. Epitaxial (205) (104) BRO thin film had a tetragonal texture whereas (110) BRO thin film showed a faceted island texture. Epitaxial (009) BRO thin films had a smooth surface due to a good lattice consistency between (009) BRO plane and (111) STO plane, and exhibited the highest electrical conductivity of $1.1 \times 10^5$ S·m$^{-1}$ among the (205) (104), (110) and (009) BRO thin films.
[doi:10.2320/matertrans.MRA2007056]

(Received March 7, 2007; Accepted April 16, 2007; Published June 20, 2007)

***Keywords:*** *laser ablation, barium ruthenate, thin films, epitaxial growth, conductive oxide, microstructure, electrical conductivity*

## 1. Introduction

Since alkaline earth metal ruthenate, $ARuO_3$ ($A$ = Ca, Sr and Ba), has an excellent chemical stability and electrical conductivity, these ruthenate are promised as an electrode and diffusion barrier material for micro devices.[1,2] The electrical conductivity of these ruthenate would be originated from hybridized orbital between Ru 4$d$ $t_{2g}$ and O 2$p$ orbital in $RuO_6$ octahedra, and then many researchers have been interested in the properties associating with the Ru 4$d$ electron.[3–5]

$CaRuO_3$ (CRO) and $SrRuO_3$ (SRO) have an orthorhombic structure which basically consists in corner-sharing $RuO_6$ octahedra.[6] On the other hand, $BaRuO_3$ (BRO) belongs to a hexagonal perovskite in which face-sharing $RuO_6$ octahedra are combined with corner-sharing $RuO_6$ octahedra. Although 9R BRO in Ramsdell notation ($R\bar{3}m$: $a = 0.575$ nm, $c = 2.161$ nm) has been commonly prepared,[6,7] 4H BRO ($P6_3/mmc$: $a = 0.574$, $c = 0.950$ nm) has been obtained as a high-pressure phase.[8,9]

Since Ru-Ru distance in BRO is significantly small due to the face-sharing octahedra, BRO exhibit characteristic electrical properties different from those of CRO and SRO, *i.e.*, 4H and 9R BRO show Fermi-liquid like behavior and a metal-insulator transition at a low temperature, respectively.[5,10–12]

Although the epitaxial growth of CRO and SRO thin films has been intensively studied, microstructure and electrical properties of BRO thin film have been scarcely reported.[13–15] In this study, BRO thin films were grown epitaxially on (001), (110) and (111) STO substrates, and the relationship among substrates, lattice consistency, microstructure and electrical conductivity was investigated.

## 2. Experimental Procedure

A third harmonic wavelength of a Q-switch pulsed Nd:YAG was used for the ablation. $RuO_2$ and $BaCO_3$ powders were used as starting materials for preparing BRO targets. These powders were weighed, mixed, pressed into pellets and reacted at 1273 K for 36.0 ks, and the BRO pellets were obtained. The BRO pellet was crashed and sintered again at 1573 K for 43.2 ks, and then the BRO target was obtained.

The deposition conditions and the details of the experimental procedure were reported elsewhere.[16,17] The deposition was carried out in $O_2$ at a pressure ($P_{O_2}$) of 13 Pa and a substrate temperature ($T_{sub}$) of 973 K. (001), (110) and (111) $SrTiO_3$ (STO) single-crystal plates ($10 \times 10 \times 0.5$ mm) were used as substrate. The BRO thin films of approximately 100 nm in thickness were obtained by the ablation for 3.6 ks.

The crystal phase was studied by X-ray diffraction (XRD, Rigaku RAD-2C). The in-plane orientation of film was determined by using pole figure X-ray diffraction (Rigaku RAD-C). The thickness was measured by a profilometer (Taylor-Hobson Talystep). The feature of film growth during the deposition was monitored using *in situ* reflection high-energy electron diffraction (RHEED). The surface morphology was observed by field-emission scanning electron microscopy (FESEM, JEOL JSM-6500FT). The electrical resistivity was measured by a van der Pauw method.

## 3. Results and Discussion

Figure 1 shows the XRD patterns of the BRO thin films prepared on various STO substrates. BRO thin films with doubly oriented to (205) and (104) (here after (205) (104)) were grown epitaxially on (001) STO substrate (Fig. 1(a)). The shape peak around $2\theta = 41.9°$ could be assigned by K$\beta$ reflection of (002) STO plane. BRO thin film with (110) and (009) orientations were grown on (110) and (111) STO substrates, respectively (Fig. 1(b), (c)).

Figure 2 shows the pole figure X-ray diffraction patterns for the epitaxial BRO thin films. The pole figure patterns for STO substrate were depicted in same figures. The four reflections from (009) BRO planes of the BRO thin film were obtained in the pole figure of the BRO thin film grown on (001) STO substrate at $\alpha = 60°$ (Fig. 2(a)). The four

*Graduate Student, Tohoku University

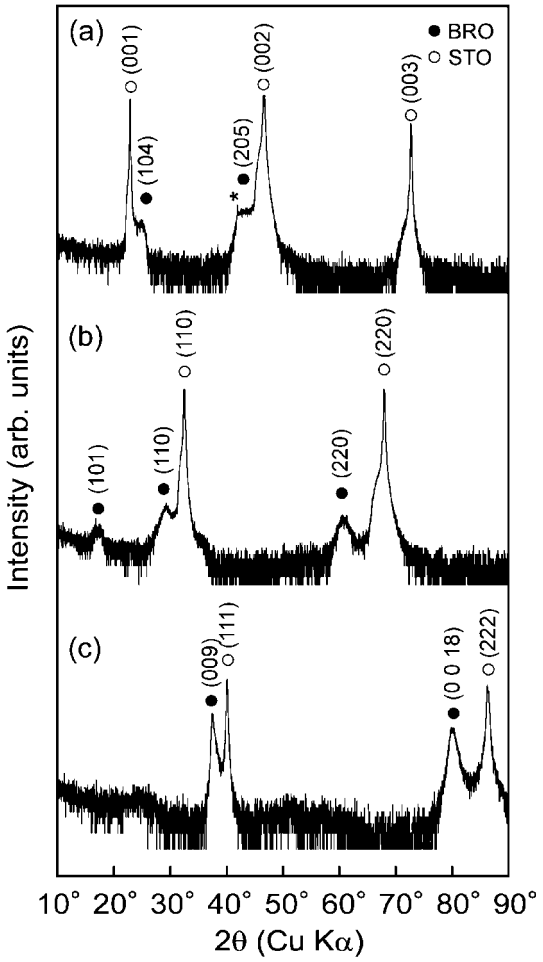


Fig. 1 XRD patterns of BRO thin films grown on (001) STO (a), (110) STO (b) and (111) STO substrates (c). K$\beta$ peak from STO substrate is indexed as an asterisk mark (*).

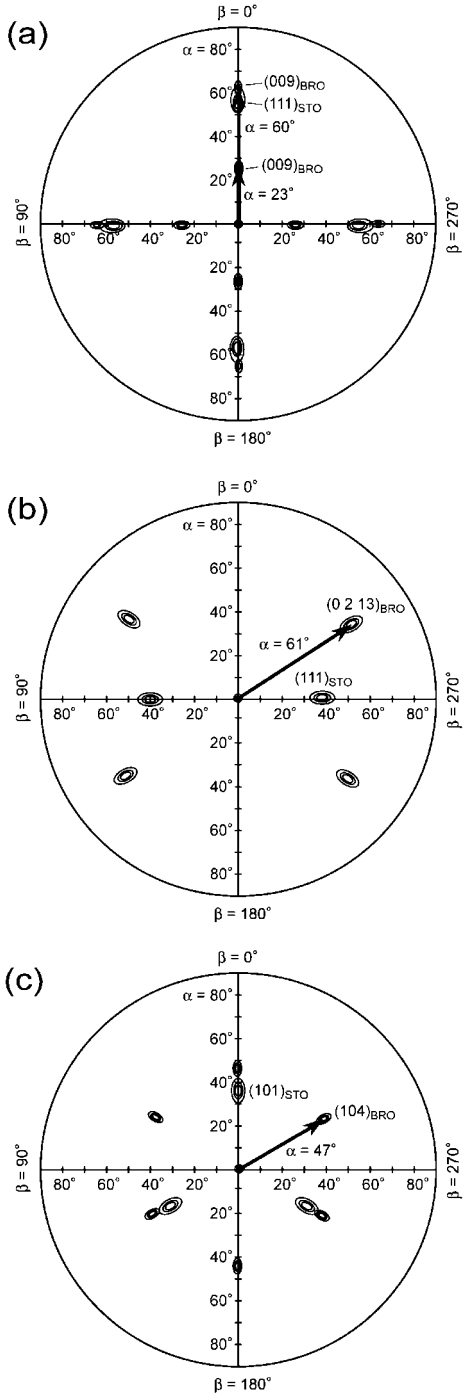


Fig. 2 X-ray pole figures for epitaxial BRO thin films: (205) (104) BRO (a), (110) BRO (b), and (009) BRO thin film (c).

reflections at $\alpha = 23^\circ$ suggest that the BRO thin film might have a small amount of (1 0 10) orientation. The four reflections from (0 2 13) BRO planes were obtained in the pole figure of the (110) BRO thin film grown on (110) STO substrate at $\alpha = 45^\circ$ and azimuthal angle of $\beta = \pm 56^\circ$ and $\pm 124^\circ$ (Fig. 2(b)). The six reflections from (104) BRO planes were obtained in the pole figure of the (009) BRO thin film grown on (111) STO substrate at $\alpha = 47^\circ$ (Fig. 2(c)). Therefore, it can be concluded that BRO thin films were epitaxially oriented to STO substrate. The pole figures of STO substrates were also measured to confirm the epitaxial relationships between thin film and substrate. The in-plane epitaxial relationship can be summarized as follows: [010] BRO // [110] STO with (205) (104) BRO/(001) STO, [$\bar{3}$31] BRO // [001] STO with (110) BRO/(110) STO and [110] BRO // [$\bar{1}\bar{1}$2] STO with (009) BRO/(111) STO.

Figure 3 shows *in situ* RHEED patterns of epitaxial BRO thin films. The incident direction of electron beam was parallel to the [110] direction for (001) STO, [001] direction for (110) STO and [$\bar{1}\bar{1}$2] direction for (111) STO. It is generally known that a streak reflection pattern in RHEED can be obtained from flat surface with a step and terrace structure whereas a spot transmission pattern can be obtained from faceted surface with an island structure.[17] The (205) (104) BRO and (110) BRO thin films showed a spot pattern, and suggesting that an island structure should be grown on the STO substrate (Fig. 3(a), 3(b)). The streak pattern of (009) BRO thin film suggests a smooth surface (Fig. 3(c)).

Figure 4 shows the surface morphology of the epitaxial BRO thin films. The (205) (104) BRO thin film had an orthogonal textured structure with rectanglarly crossed tetragonal grains on the (001) STO substrate (Fig. 4(a)). The (110) BRO thin film of faceted elongated plate-like grains was grown in two directions on the (110) STO substrate (Fig. 4(b)). The (009) BRO thin film with a flat and smooth surface with round-shaped hexagonal grains of about 50 nm in diameter was observed on the (111) STO substrate

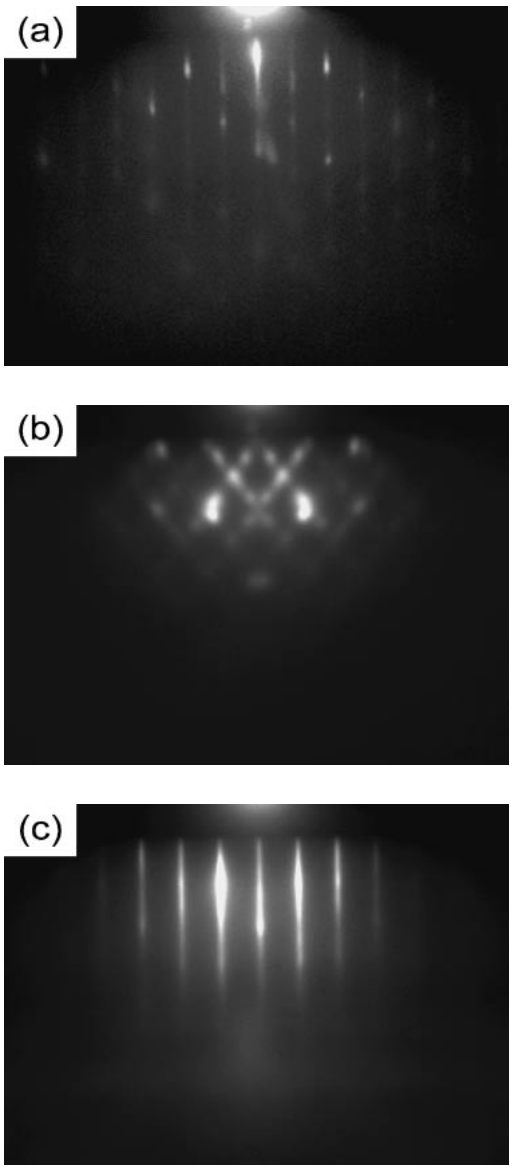


Fig. 3 *in situ* RHEED diffraction patterns of epitaxial BRO thin films grown on various STO substrates. Incidence direction of electron beam is $\langle 100 \rangle$ for (001) STO (a, b), $\langle 00\bar{1} \rangle$ for (110) STO (c, d), and $\langle 11\bar{2} \rangle$ for (111) STO substrates.

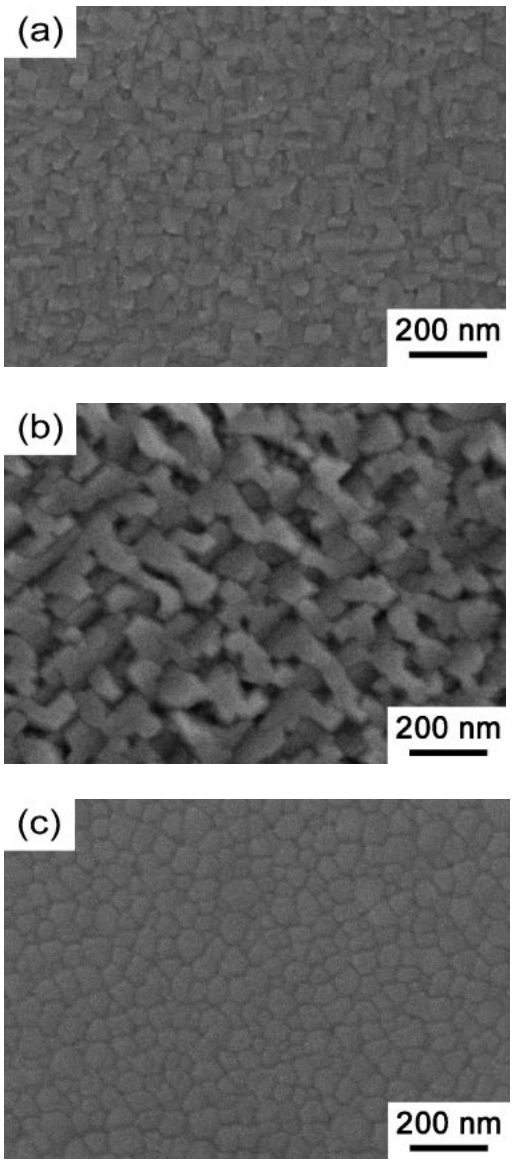


Fig. 4 Plan-view FESEM images of epitaxial BRO thin films grown on (001) STO (a), (110) STO (b) and (111) STO substrates (c).

(Fig. 4(c)). These results were in agreement with the RHEED observation that the spot and streak patterns imply the island and smooth textures, respectively.

It was reported that (205) BRO plane can be epitaxially grown on the (001) STO and (001) $LaAlO_3$ substrate.[13–15,18] In this study, (104) BRO plane was also epitaxially grown on the (001) STO substrate (Fig. 1(a)). Figure 5 demonstrates the schematic plan-views of (205) BRO and (104) BRO planes on (001) STO. The (205) BRO plane is a slightly distorted tetragonal lattice consisting of Ba and Ru atoms (Fig. 5(a)), and good consistency with (001) STO lattice as shown as shaded regions with misfit ratio ($r_{misfit}$) of 5.8%. The (104) BRO plane also has similar lattice to (205) BRO plane ($r_{misfit} = 5.8\%$), and may have slightly greater mismatch for the epitaxial growth than (205) BRO plane (Fig. 5(b)). These lattice consistency of both (205) and (104) BRO planes could coincide well with the orthogonal textured surface morphology as shown in Fig. 4(a). Therefore, (104) BRO plane can be also an epitaxial plane for the thin film grown on (001) STO substrate. Figure 6 shows a plan-view of (110) BRO plane on (110) STO. A part of Ru and Ti octahedra was described for simplicity. (110) BRO plane has good lattice consistency with (110) STO substrate ($r_{misfit} = 6.7\%$) along with $\langle 1\bar{1}0 \rangle$ and $\langle \bar{1}10 \rangle$ BRO direction (shaded regions in Fig. 6). Figure 7 shows a plan-view of (009) BRO plane on (111) STO substrate. (009) BRO plane has excellent lattice consistency with (111) STO plane ($r_{misfit} = 3.8\%$), and then the (009) BRO grains could grow along *c*-axis with a smooth surface.

Figure 8 shows the temperature dependence of electrical resistivity of the epitaxial (205) (104), (110) and (009) BRO thin films. Each epitaxial thin film has metallic conduction. The epitaxial (009) BRO thin film exhibited the highest electrical conductivity at room temperature of $1.1 \times 10^5$ $S \cdot m^{-1}$ among the (205) (104), (110) and (009) BRO thin films. The surface morphology might be associated with the

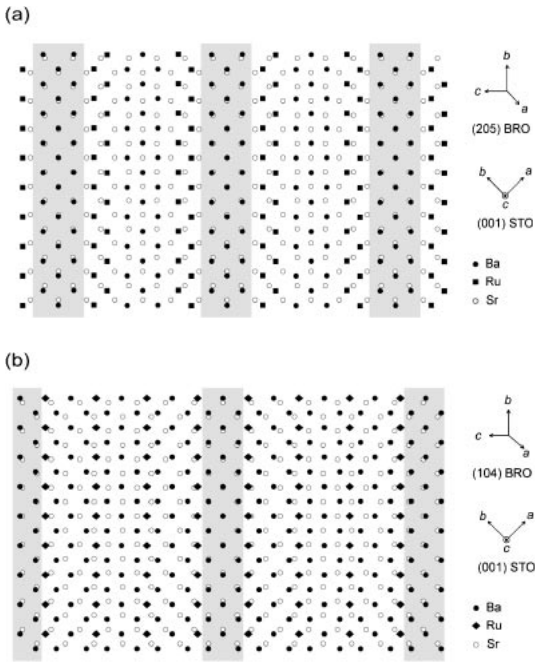


Fig. 5 Schematic plan-view of (205) BRO (a) and (104) BRO planes (b) on (001) STO. Shaded regions indicate good lattice consistency areas.

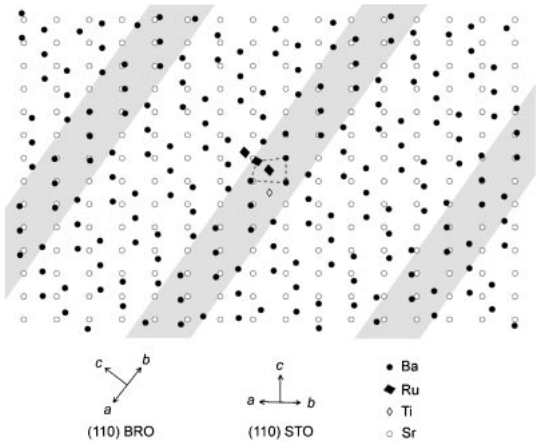


Fig. 6 Schematic plan-view of (110) BRO plane on (110) STO. Shaded regions indicate good lattice consistency areas.

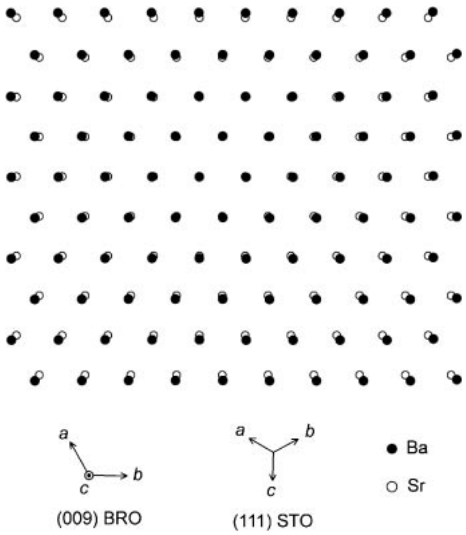


Fig. 7 Schematic plan-view of (009) BRO plane on (111) STO.

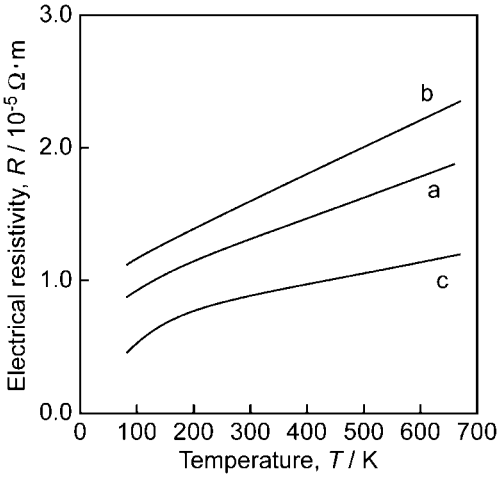


Fig. 8 Temperature dependence of electrical resistivity of epitaxial BRO thin films grown on (001) STO (a), (110) STO (b) and (111) STO substrates (c).

electrical resistivity, where the smooth surface of (009) BRO thin film had higher conductivity than the faceted surface of (205) (104) and (110) BRO thin film. It was reported that the electrical conduction behavior could be related with the polytypism of BRO particularly at a low temperature. 4H BRO shows a Fermi-liquid like $T^2$ dependence of electrical resistivity,[11,12] whereas 9R BRO has a metal-insulator transition with a large resident resistivity.[12] Table 1 summarized that the literature data on the structural and electrical properties for 4H and 9R BRO single crystals and epitaxial BRO thin films.[5,11–15,19,20] For single crystals, a anisotropical temperature dependence of electrical resistivity between in-plane (*ab*) and out-of-plane (*c*) was observed only in 9R BRO.[12] This difference between 4H and 9R BRO might be caused by a variation from stacking sequence of face-sharing octahedra with small Ru-Ru distance. The electrical conductivity of epitaxial BRO thin films prepared in this study was almost as the same order as that of single crystal. Lee *et al.* reported that $(02\bar{2}3)$-oriented 4H BRO thin film with a minor amount of (205) 9R BRO thin film was grown epitaxially on (001) STO substrate.[15] On the other hand, doubly oriented (205) and (104) BRO thin film was obtained in this study. Although (205) 9R BRO thin film was commonly prepared on (001) STO substrate, another plane can be also an epitaxial plane. The surface morphology and electrical conductivity of epitaxial (110) BRO thin film grown on (110) STO substrate was first revealed. In both cases of 4H or 9R BRO thin film, columnar crystal grains could grow along *c*-axis with a smooth terrace structure on (111) STO substrate.[19] These *c*-axis oriented BRO thin films exhibited a higher electrical conductivity than that of the epitaxial thin films with another orientation in both films prepared by sputtering and PLD (laser ablation). This highly conductivity could be caused by a small mismatch between film and substrate.

Table 1 Literature data on the structural and electrical properties of single crystal BRO and epitaxial BRO thin films prepared on STO substrates.

| Methods | Substrate | Crystal structure and film orientation | Surface morphology | Resistivity [Ω·m] | Ref. |
|---|---|---|---|---|---|
| **Single crystal** | | | | | |
| Solid state reaction | | 9R | — | $1.0 \times 10^{-6}$ | 5) |
| Flux | | 9R | Rhombic basal plane | $3.5 \times 10^{-6}$ (*ab*)<br>$1.6 \times 10^{-6}$ (*c*) | 12) |
| | | 4H | Hexagonal basal plane | $4.0 \times 10^{-6}$ (*ab*)<br>$5.5 \times 10^{-6}$ (*c*) | |
| **Epitaxial thin film** | | | | | |
| PLD | (001) STO | (205) 9R | — | $1.0 \times 10^{-5}$ | 14) |
| Sputtering | (001) STO | (205) 9R | — | $7.6 \times 10^{-6}$ | 13,14,20) |
| Sputtering | (001) STO | $(02\bar{2}3)$ 4H | Orthogonal texture | $9.9 \times 10^{-6}$ | 15) |
| PLD | (001) STO | (205) (104) 9R | Orthogonal texture | $1.3 \times 10^{-5}$ | This work |
| PLD | (110) STO | (110) 9R | Plate-like island | $1.5 \times 10^{-5}$ | This work |
| Sputtering | (111) STO | 4H | — | $6.0 \times 10^{-6}$ | 11) |
| Sputtering | (111) STO | (004) 4H | Concentric terrace | $8.1 \times 10^{-6}$ | 19) |
| PLD | (111) STO | (009) 9R | Hexagonal terrace | $8.7 \times 10^{-6}$ | This work |

PLD: pulsed laser deposition (laser ablation)

## 4. Conclusions

BRO thin films were prepared on STO single crystal substrate by laser ablation, and (205) (104), (110) and (009) BRO thin films were grown epitaxially with in-plane orientations on (001), (110) and (111) STO substrate, respectively. The in-plane epitaxial relationships were as follows: [010] BRO // [110] STO with (205) (104) BRO/(001) STO, $[\bar{3}31]$ BRO // [001] STO with (110) BRO/(110) STO and [110] BRO // $[\bar{1}\bar{1}2]$ STO with (009) BRO/(111) STO. Tetragonal textured (205) (104) BRO and faceted plate-like (110) BRO thin films were grown epitaxially on (001) and (110) STO substrate, respectively, whereas flat and smooth textured (009) BRO thin films grown epitaxially on (111) STO substrate. The *in situ* RHEED observation corresponded well with the surface morphology. The epitaxial (009) BRO thin film exhibited the highest electrical conductivity of $1.1 \times 10^5\,S \cdot m^{-1}$ among the (205) (104), (110) and (009) BRO thin films.

## Acknowledgements

This research was supported in part by the 21 century COE program of Tohoku University. This research was also supported in part by the Asian CORE program, Japan Society for the Promotion of Science (JSPS). We are grateful to Y. Hayasaka and E. Aoyagi, Institute for Materials Research, for FESEM observation. This research was financially supported in part by Furuya metal Co., Ltd. and Lonmin Plc.

## REFERENCES

1) K. Char, M. S. Colclough, T. H. Geballe and K. E. Myers: Appl. Phys. Lett. **62** (1993) 196–198.
2) T. Morimoto, O. Hidaka, K. Yamakawa, O. Arisumi, H. Kanaya, T. Iwamoto, Y. Kumura, I. Kunishima and S. Tanaka: Jpn. J. Appl. Phys. **39** (2000) 2110–2213.
3) A. Callaghan, C. W. Moeller and R. Ward: Inorg. Chem. **5** (1966) 1572–1576.
4) M. V. R. Rao, V. G. Sathe, D. Sornadurai, B. Panigrahi and T. Shripathi: J. Phys. Chem. Solids **62** (2001) 797–806.
5) M. Shepard, S. McCall, G. Cao and J. E. Crow: J. Appl. Phys. **81** (1997) 4978–4980.
6) J. J. Randall and R. Ward: J. Amer. Chem. Soc. **81** (1959) 2629–2631.
7) P. C. Donohue, L. Katz and R. Ward: Inorg. Chem. **4** (1965) 306–310.
8) S.-T. Hong and A. W. Sleight: J. Solid State. Chem. **128** (1997) 251–255.
9) J. M. Longo and J. A. Kafalas: Mater. Res. Bull. **3** (1968) 687–692.
10) C. Felser and R. J. Cava: Phys. Rev. B **61** (2000) 10005–10009.
11) Y. S. Lee, J. S. Lee, K. W. Kim, T. W. Noh, J. Yu, Y. Bang, M. K. Lee and C. B. Eom: Phys. Rev. B **64** (2001) 165109.
12) J. T. Rijssenbeek, . Jin, Y. Zadorozhny. Y. Liu, B. Batlogg and R. J. Cava: Phys. Rev. B **59** (1999) 4561–4564.
13) N. Fukushima, K. Sano, T. Schimizu, K. Abe and S. Komatsu: Appl. Phys. Lett. **73** (1998) 1200–1202.
14) J. Lettieri, I. W. Scrymgeour, D. G. schlom, M. K. Lee and C. B. Eom: Appl. Phys. Lett. **77** (2000) 600–601.
15) M. K. Lee, C. B. Eom, J. Lettieri, I. W. Scrymgeour, D. G. Schlom, W. Tian, X. Q. Pan, P. A. Ryan and F. Tsui: Appl. Phys. Lett. **78** (2001) 329–331.
16) A. Ito, H. Masumoto and T. Goto: Mater. Trans. **47** (2006) 2808–2814.
17) A. Ito, H. Masumoto and T. Goto: Mater. Trans. **48** (2007) 227–233.
18) D. Kaur and K. V. Rao: Solid State Comm. **128** (2003) 391–395.
19) M. K. Lee, C. B. Eom, W. Tian, X. Q. Pan, M. C. Smoak, F. Tsui and J. J. Krajewski: Appl. Phys. Lett. **77** (2000) 364–366.
20) N. Fukushima, K. Sano, T. Schimizu, K. Abe, S. Komatsu and S. Takeno: Appl. Phys. Lett. **77** (1998) 600–601.